CENTRE DE RECERCA MATEMÀTICA

Preprint núm. 1152
April 2013

Continuum mathematics at the nanoscale

T.G. Myers, M.M. MacDevette, F. Font

CONTINUUM MATHEMATICS AT THE NANOSCALE

ABSTRACT. In this paper we discuss three examples where continuum theory may be applied to describe nanoscale phenomena:

1. Enhanced flow in carbon nanotubes (CNTs) – This model shows that the experimentally observed enhancement can be explained using standard flow equations but with a depletion layer between the liquid and solid interfaces.
2. Nanoparticle melting – Nanoparticles often exhibit a sharp increase in melting rate as the size decreases. A mathematical model will be presented which predicts this phenomena.
3. Nanofluids – Experimental results concerning the remarkable heat transfer characteristics of nanofluids are at times contradictory. We develop a model for the thermal conductivity of a nanofluid, which provides much higher predictions than the standard Maxwell model and a better match to data.

1. INTRODUCTION

Continuum theory may be applied when there is a sufficently large sample size to ensure that statistical variation of material quantities, such as density, is small. For fluids the variation is often quoted as 1% [1]. Assuming a spherical sample Nguyen and Werely [2] suggest this level of variation requires a minimum of 10^4 atoms and so deduce a critical dimension of the order 10 and 90nm for liquids and gases respectively. In fact by comparing molecular dynamics simulations to computations based on the Navier-Stokes equations Travis *et al* [4] show that continuum theory may be applied to water flow down to around 3nm. Thomas et al [6] suggest a figure of 1.66nm. In the field of heat transfer and phase change it has been suggested that continuum theory requires particle radii greater than 2nm [3]. Kofman *et al* [7] state that at scales smaller than 5nm the melting process is discontinuous and dominated by fluctuations, Kuo *et al* [8] observed structural changes and a 'quasi-molten' state in their study of nanoparticle melting between 2-5nm.

Nanoscale is typically described as involving materials with at least one dimension below 100nm [9], so there is clearly a range of sizes where continuum theory may be applied to nano phenomena. In this paper we will apply continuum theory to problems in fluid and heat flow and demonstrate how seemingly anomalous behaviour may be explained without resorting to molecular dynamics or empirically based adjustments. In §2 we employ a concept from non-Newtonian fluid dynamics, that of a bi-viscosity fluid, to explain why observed flow rates of water in carbon nanotubes are much higher than that predicted by classical theory. The model also suggests a physical interpretation for the Navier slip condition. In §3 we investigate the melting

Key words and phrases. carbon nanotubes, enhanced flow, nanoparticle melting, thermal conductivity, nanofluid.

CRM Preprint Series number 1152

of nanoparticles. As the particles decrease in size, and so the ratio of bulk to surface atoms decreases, it becomes easier for surface atoms to leave the particle. This results in a decrease in the melt temperature. Using a form of the Gibbs-Thompson relation to describe the variation of melt temperature with size we produce a model that explains the experimentally observed 'abrupt melting'. Finally, in §4 we investigate the thermal conductivity of nanofluids (a nanofluid is a fluid containing nanoparticles). The classical Maxwell model to describe the heat conduction of a solid in liquid suspension is known to significantly underpredict the thermal response of a nanofluid. The Maxwell model is based on a static analysis. Using an approximate solution method to the heat flow problem we obtain an expression for the thermal conductivity of the fluid which shows much better agreement with experiment.

2. Enhanced Flow In Carbon Nanotubes (CNTs)

Carbon nanotubes are a cylindrical nanostructure formed from graphene. They have unusual properties: they are extremely good at conducting heat and electricity and have remarkable strength. Consequently there is intensive research into their uses and there is a wide variety of suggested applications. One application, in textiles, is based on the observation that CNTs transport water at a much faster rate than predicted by classical flow theory. Papers in *Nature* and *Science* [10, 11] reported increases by orders of magnitude, although recent work provides more conservative estimates: Whitby *et al* [12] quote a maximum increase by a factor of 45.

The classical model for flow in a circular cylindrical pipe is described by the Hagen-Poiseuille equation which leads to an expression for the fluid flux:

$$Q_{HP} = -\pi R^4 p_z/(8\mu)\,, \tag{1}$$

where p_z is the pressure gradient along the pipe, R is the radius and μ the fluid viscosity. In CNTs it is well documented that the flux is significantly higher than this value.

A popular approach to explain this enhancement is to introduce a slip-length into the mathematical model, that is, the no-slip boundary condition $u(R) = 0$ is replaced by

$$u(R) = -L_s \frac{\partial u(R)}{\partial r} \tag{2}$$

where L_s is the slip-length and u the velocity. This leads to a modified flux expression

$$Q_{slip} = Q_{HP}\left(1 + \frac{4L_s}{R}\right). \tag{3}$$

The literature typically discusses flow enhancement, which is defined as the ratio of the observed to predicted fluxes, $\varepsilon_{slip} = Q_{slip}/Q_{HP}$. Clearly any magnitude of enhancement can be accounted for by using an appropriate value for L_s. Comparison of theory with experiments on the microscale leads to sensible values of the slip length, which are much smaller than the channel dimension. Yet, when dealing with nanochannels

CRM Preprint Series number 1152

the slip lengths are typically on the order of microns. There is no theory to predict the slip length for a liquid flowing past a solid however, there is one for gases. In this case, the slip length is of the order of the mean free path of the gas [13] (for water the mean free path is 0.3 nm). To match their experimental observations Holt *et al*. [10] and Majumder *et al*. [11] quote slip lengths on the order of microns. Of course the high values of slip-length in CNT studies have led some authors to question the validity of the slip modified Hagen-Poiseuille model [14, 15]. Cottin-Bizonne *et al.* [17] state that the slip-length should have a single value independent of the tube radius and much less than those quoted in the literature. They attribute some of the high experimental values to contamination by hydrophobic particles.

An alternative explanation to the slip-length is based on the fact that CNTs are hydrophobic. The strength of attraction between water molecules is greater than the attraction between the hydrophobic solid and the water [18]. It has been postulated that hydrophobicity may result in gas gaps, depletion layers or the formation of vapour: all descriptions result in a region of low viscosity close to the wall and experimentally this may be interpreted as 'apparent' slippage [19, 18]. Poynor *et al* [16] state that their synchrotron x-ray data unambiguously demonstrates a depletion layer is formed when water meets a hydrophobic surface. Depletion layers have also been predicted via molecular dynamics (MD) simulations [20]. Joseph and Aluru [21] observed a hydrogen bonding depletion layer, Barrat and Bocquet [23] show that the first layer of water molecules is depleted in the presence of a hydrophobic wall.

Assuming the presence of a depletion layer standard fluid equations may be employed using a bi-viscosity model, with a bulk flow region occupying the centre of the channel and a depleted region with low viscosity near the walls. If the velocity and shear stress are matched at the interface, defined by $r = \alpha$, then the flux is

$$Q_\mu = Q_{HP}\frac{\alpha^4}{R^4}\left(1+\frac{\mu_1}{\mu_2}\left(\frac{R^4}{\alpha^4}-1\right)\right), \tag{4}$$

where μ_1, μ_2 represent the bulk and depletion layer viscosities respectively, $\mu_1 \gg \mu_2$ and α is the radius of the bulk region (for CNTs experiments indicate a depletion layer thickness $\delta = 0.7$nm, hence $\alpha = R - 0.7$nm). The flow enhancement is defined as the ratio $\varepsilon_\mu = Q_\mu/Q_{HP}$. Taking data from [12] it turns out that $\mu_2 \approx 0.018\mu_1$. The viscosity of air and oxygen are approximately 0.02 that of water. Obviously these are two readily available gases, the air could be entrained somehow or dissolved in the water, the oxygen is already contained in the water.

With gas flow there is a theory to account for apparent slip over a solid surface however no such theory has been found for fluids. Comparison of the above flux expressions with slip and a depletion layer leads to an expression for an effective slip-length for a fluid

$$L_s = \delta\left(\frac{\mu_1}{\mu_2}-1\right)\left[1-\frac{3}{2}\frac{\delta}{R}+\left(\frac{\delta}{R}\right)^2-\frac{1}{4}\left(\frac{\delta}{R}\right)^3\right]. \tag{5}$$

CRM Preprint Series number 1152

This is a monotonically decreasing function of R (as predicted by Thomas & McGaughey [14]). Further, noting that $\mu_1/\mu_2 \gg 1$, we can identify three distinct regimes:

1. For sufficiently wide tubes, such that $\delta/R \ll \mu_2/\mu_1$, then $\varepsilon_\mu \approx 1$. There is no noticeable flow enhancement and the no-slip boundary condition will be sufficient, $L_s \approx 0$. This should hold approximately for $R > 3\mu$m. On smooth surfaces slip is not observed in wide tubes.

2. For moderate tubes, such that $(\delta/R)(\mu_1/\mu_2)$ is order 1 but $\delta/R \ll 1$ then only the leading order term of L_s applies and

$$\varepsilon_\mu \approx 1 + \frac{4\delta}{R}\left(\frac{\mu_1}{\mu_2} - 1\right). \tag{6}$$

This holds approximately for $R \in [21\text{nm}, 3\mu\text{m}]$ and corresponds to a constant slip length, $L_s = \delta\mu_1/\mu_2$. It holds for approximately $R \in [21\text{n}m, 3\mu\text{m}]$. Numerous papers report constant slip-lengths around 20-40nm [17, 22] (for $R \in$ 'some nanometers up to several hundreds of nanometers').

3. For very small tubes where δ/R is order 1 then the full expression for ε_μ is required and the slip length varies with tube radius. Thomas *et al* [6] suggest L_s varies with R for $R \in [1.6, 5]$nm and show $\varepsilon \approx 32$ when $R = 3.5$nm. The above model predicts $\varepsilon \approx 33.2$ for this R value. It also predicts a maximum enhancement (obtained by setting $R = \delta$) of around 50 which compares well with the maximum value of 45 observed by Whitby *et al* [12].

If we define an average viscosity, say by equating fluxes from a bi-viscosity and single viscosity model, then it is clear that μ_{av} decreases with tube radius (since the depletion region will occupy a larger proportion of the tube as R decreases). This is in agreement with MD simulations see, for example, [24, 6].

3. NANOPARTICLE MELTING

Nanomaterials are currently the subject of intense investigation due to their unique properties and a wide range of novel applications such as in optical, electronic, catalytic and biomedical applications, single electron tunneling devices, nanolithography *etc* [25, 26, 27]. One reason for their interesting behaviour is that they have a very large ratio of surface to volume atoms which can have a significant effect on the material properties [3]. A particular example of this is the well-documented decrease in phase change temperature as the material dimensions decrease [27]. The experiments of Buffat and Borel [39] show a decrease of around 500K for gold particles with radius slightly greater than 1nm. The molecular dynamics simulations of Shim *et al* [27] show a decrease of more than 800K below the bulk melt temperature (a 40% decrease) for gold nanoparticles with a radius around 0.8 nm. Drugs with poor water solubility may be administered as nanoparticles to improve their uptake. Bergese *et al* [28] and Liu *et al* [40] study antibiotic and antianginal drugs, which exhibit a melting point depression of around 30K (a 10% decrease from the bulk value). Since gold has low

CRM Preprint Series number 1152

toxicity, gold nanoparticles also make good carriers for drug and gene delivery [29]. Many applications require the particles to melt, after serving their primary purpose, and so pass through the system as disperse molecules. Hence it is important to understand the thermal response of a nanoparticle and its likely phase change behaviour.

If the density and specific heat remain approximately constant in each phase the melt temperature may be estimated from the following generalised Gibbs-Thomson relation

$$L_m\left(\frac{T_m}{T_m^*}-1\right)+\Delta c\left[T_m\ln\left(\frac{T_m}{T_m^*}\right)+T_m^*-T_m\right]=-\frac{2\sigma_{sl}\kappa}{\rho_s} \tag{7}$$

where L_m is the latent heat, T_m is the temperature at which the phase change occurs, T_m^* the bulk phase change temperature, $\Delta c = c_l - c_s$ the change in specific heat from liquid to solid, σ the surface tension and κ the mean curvature. Note, it is assumed that the ambient pressure variation is small, so a term related to pressure effects on the temperature has been neglected. Figure 1 compares results for the generalised Gibbs-Thomson relation against experiment for gold nanoparticles between 2 and 12 nm, see [38].

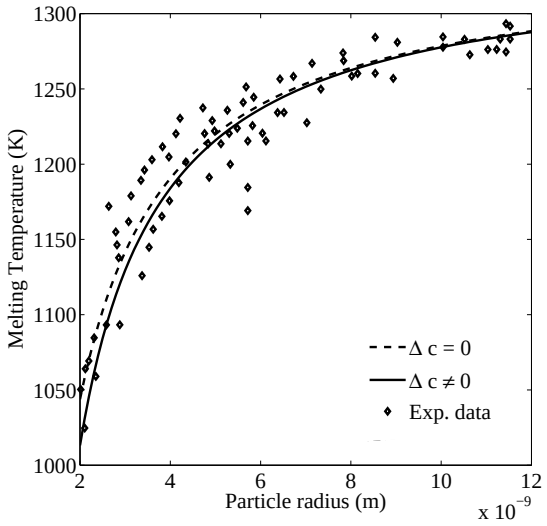

FIGURE 1. Variation of the melt temperature of gold nanoparticles

An appropriate non-dimensional mathematical model for the melting of a spherically symmetric particle is given by

$$\frac{\partial T}{\partial t}=\frac{1}{r^2}\frac{\partial}{\partial r}\left(r^2\frac{\partial T}{\partial r}\right),\qquad \frac{\partial \theta}{\partial t}=\frac{k}{c}\frac{1}{r^2}\frac{\partial}{\partial r}\left(r^2\frac{\partial \theta}{\partial r}\right) \tag{8}$$

CRM Preprint Series number 1152

where T, θ represent the temperature in the liquid and solid respectively. The boundary conditions are $T(1,t) = 1$, $T(R,t) = \theta(R,t) = T_m$, $\theta_r(0,t) = 0$ and the Stefan condition

$$[\beta + (1-c)T_m]\frac{dR}{dt} = k\frac{\partial\theta}{\partial r} - \frac{\partial T}{\partial r}\bigg|_{r=R}. \tag{9}$$

The nondimensional melting temperature T_m is determined from

$$0 = \beta\left(T_m + \frac{\Gamma}{R}\right) + \frac{(1-c)}{\delta T}\left[\left(T_m + \frac{1}{\delta T}\right)\ln\left(T_m\,\delta T + 1\right) - T_m\right]. \tag{10}$$

The dimensionless parameters above are defined by

$$\alpha_l = k_l/\rho_l c_l \qquad c = c_s/c_l \qquad k = k_s/k_l$$
$$\beta = L_m/c_l\Delta T \qquad \delta T = \Delta T/T_m^* \qquad \Gamma = 2\sigma_{sl}T_m^*/R_0\rho_l L_m\Delta T.$$

For a temperature increase of $\Delta T = 10$K we have $\beta \approx 8$, 40, 12 for water, gold and lead, respectively. Obviously, the smaller the increase ΔT the larger the value of β. Due to the small volume of the nanoparticles the energy required to melt them is also small: any increase above the melting temperature, ΔT, on the nanoparticle surface is enough to almost instantaneously melt it. Hence, working in a large Stefan number regime, where $\beta \gg 1$, is a sensible assumption. Note, small β indicates a fast melting process as the temperature applied at the nanoparticle surface, T_H, is much greater than the melting temperature, T_m, large β implies a slower process as T_H is closer to T_m (although given that the time-scales are on the order of pico seconds slow and fast are relative terms). This suggests a link between β and the time-scale, hence we re-scale time as $t = \beta\tau$ and look for solutions of the form $T = T_0 + T_1/\beta + \cdots$. In the liquid we find

$$\mathscr{O}(1): \qquad 0 = \frac{1}{r^2}\frac{\partial}{\partial r}\left(r^2\frac{\partial T_0}{\partial r}\right), \qquad T_0(1,\tau) = 1, \qquad T_0(R,\tau) = T_m \tag{11}$$

$$\mathscr{O}(1/\beta): \qquad \frac{\partial T_0}{\partial\tau} = \frac{1}{r^2}\frac{\partial}{\partial r}\left(r^2\frac{\partial T_1}{\partial r}\right), \qquad T_1(1,\tau) = 0, \qquad T_1(R,\tau) = 0 \tag{12}$$

with respective solutions

$$T_0 = 1 + (T_m - 1)\frac{R}{r}\left(\frac{1-r}{1-R}\right) \tag{13}$$

$$T_1 = \mu_1\left\{\left[(3-r)r - \frac{2}{r}\right] - \frac{R}{r}\left(\frac{1-r}{1-R}\right)\left[(3-R)R - \frac{2}{R}\right]\right\}\frac{dR}{d\tau} \tag{14}$$

where

$$\mu_1 = \left[\frac{\beta\Gamma}{R\left[\beta + \frac{(1-c)}{\delta T}\ln\left(T_m\delta T + 1\right)\right]} + \frac{(T_m - 1)}{(1-R)}\right]. \tag{15}$$

In the solid

$$\theta_0 = T_m, \qquad \theta_1 = -\mu_2(R^2 - r^2)\frac{dR}{d\tau} \tag{16}$$

CRM Preprint Series number 1152

where

$$\mu_2 = \frac{c}{6k}\frac{\beta\Gamma}{R^2\left[\beta + \frac{(1-c)}{\delta T}\ln\left(T_m\delta T + 1\right)\right]}. \tag{17}$$

The Stefan condition is

$$\frac{dR}{d\tau} = \frac{(T_m - 1)}{R(1-R)}\left[1 + \frac{1}{\beta}\left((1-c)T_m - 2\mu_1\frac{(1-R)^2}{R} - 2k\mu_2 R\right)\right]^{-1} \tag{18}$$

and this is coupled to the differentiated form of the Gibbs-Thomson equation

$$\frac{dT_m}{d\tau} = \frac{\Gamma}{R^2\left[+\frac{(1-c)}{\beta\delta T}\ln\left(T_m\delta T + 1\right)\right]}\frac{dR}{d\tau}. \tag{19}$$

These equations are subject to $R(0) = 1$ and $T_m(0) = T_m(1)$ (this value is determined by solving (10) with $R = 1$). Hence, the original system, consisting of heat equations in the solid and liquid defined over a changing domain which is specified by the Stefan condition and coupled to an equation describing the phase change temperature has now been reduced to solving two first order ODEs.

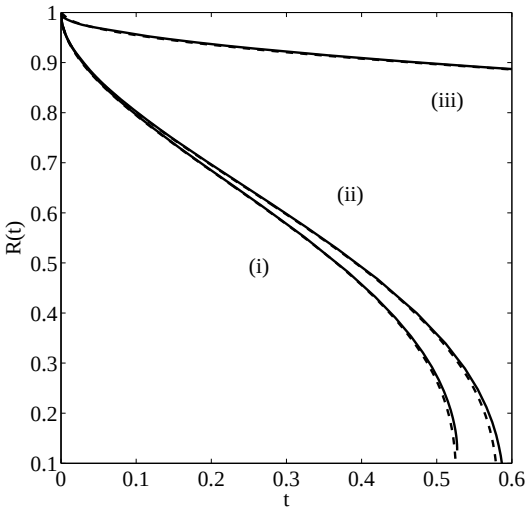

FIGURE 2. Typical result for non-dimensional position of melt front $R(t)$ (to convert to dimensional form multiply R by the original particle radius of 10nm and t by the time-scale 2.7ps)

In Figure 2 we show the evolution of the melt front, $R(t)$, with time. The dashed lines are the approximate solution, the solid lines come from a numerical solution of the full system. The three sets of curves represent three solution forms, the curves labelled (i) represent the model using the generalised Gibbs-Thomson relation, curves (ii) take $c_s = c_l$ in Gibbs-Thomson but not the energy balance (this is the form used in [30])

CRM Preprint Series number 1152

and curves (iii) are the standard model where $c_s = c_l$ and $T_m = T_m^*$. It is clear that the standard model will overpredict the melt time by a significant amount (usually at least by an order of magnitude). Curves (i) and (ii) demonstrate how, as the solid radius decreases, the gradient of the curve increases and tends to infinity. So, in the final stages of melting it is predicted that the particle will suddenly disappear. This is the 'abrupt melting' phenomena observed by [7]. Figure 3 shows the temperature profile within the liquid and solid regions as the particle melts. The dotted line indicates how the melt temperature decreases with time, the dashed line is the temperature in the solid phase, the solid line the temperature in the liquid.

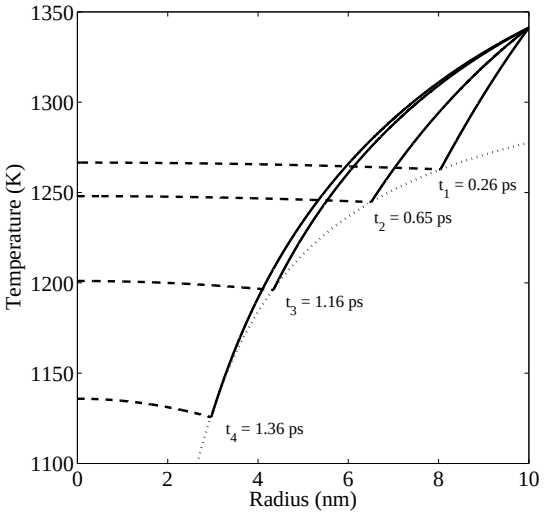

FIGURE 3. Temperature profiles within a melting nanoparticle

4. THERMAL CONDUCTIVITY OF NANOFLUIDS

There exists a vast literature on the enhanced thermal properties of nanofluids when compared to their base fluids (a nanofluid fluid is a fluid containing nanoparticles [9]). The often remarkable enhancement then suggests nanofluids as the solution for heat removal in many modern electronic devices. However there are discrepancies and much debate over experimental findings and so far no satisfactory mathematical model has been proposed to describe the thermal response of a nanofluid [31, 32].

The classical analysis of heat conduction for solid-in-liquid suspensions is that of Maxwell, based on effective medium theory. This leads to an expression for the effective thermal conductivity

$$\frac{k_e}{k_l} = \left[\frac{2k_l + k_p + 2\phi(k_p - k_l)}{2k_l + k_p - \phi(k_p - k_l)} \right], \tag{20}$$

CRM Preprint Series number 1152

where k_e, k_p, k_l represent the effective, particle and liquid thermal conductivity and ϕ is the particle volume fraction. There are obvious problems with the Maxwell model. Firstly, it is based on analysing the heat flow in the material surrounding an equivalent nanofluid and the heat flow around a particle, as opposed to analysing the actual nanofluid or particle behaviour. The analysis is carried out over an infinite region [9]. Hence the result can only be applied to a highly disperse fluid where the particles are so far apart that an energy change in one has a negligible effect on any other particle. This approach will clearly lead to problems as the particle concentration increases. Further, the Maxwell model is based on a steady-state solution but in general one would wish to analyse how a nanofluid responds in a time-dependent situation.

Keblinski *et al* [41] compared the data from various groups working with nanofluids and found that for most of the data $k_e \approx (1 + C_k\phi)k_l$ with $C_k \approx 5$ whilst the linearised Maxwell model predicts $C_k \approx 3$. In an attempt to improve the fit between theory and experiment various researchers have extended or modified Maxwell's model to account for nanolayers, particle clustering, nanoconvection and Brownian motion. Examples of these include the work of Koo and Kleinstreuer [33] who alter the Maxwell model by adding on a term to account for Brownian motion. Prasher *et al* [32] multiply the Maxwell result to include a Brownian factor. Yu et al [34] use a nanolayer (a thin layer of ordered liquid molecules surrounding the particle) with thickness 2nm and a conductivity greater than ten times that of the base fluid. In [9] a comprehensive list of variations to Maxwell's model and similar theories are described. In each case the introduction of new effects and new parameters permits better agreement with certain experiments.

Working with the diffusion time-scale in the liquid an appropriate non-dimensional model for heat flow through a spherically symmetric liquid-particle system may be written

$$\frac{\partial T}{\partial t} = \frac{\alpha}{r^2}\frac{\partial}{\partial r}\left(r^2\frac{\partial T}{\partial r}\right) \qquad r \in [0, r_p] \tag{21}$$

$$\frac{\partial \theta}{\partial t} = \frac{1}{r^2}\frac{\partial}{\partial r}\left(r^2\frac{\partial \theta}{\partial r}\right) \qquad r \in [r_p, 1]\,, \tag{22}$$

where $\alpha = \alpha_p/\alpha_l$ is the ratio of thermal diffusivities and r_p the particle radius. Imposing continuity of temperature and heat flux at the fluid-particle interface and a fixed boundary temperature greater than the initial temperature appropriate boundary conditions are

$$\theta(r,0) = T(r,0) = 0 \qquad \theta(1,t) = 1 \qquad \theta(r_p,t) = T(r_p,t) = T_p(t) \tag{23}$$

$$\left.\frac{\partial \theta}{\partial r}\right|_{r=r_p} = k\left.\frac{\partial T}{\partial r}\right|_{r=r_p} \qquad \left.\frac{\partial T}{\partial r}\right|_{r=0} = 0\,, \tag{24}$$

where $k = k_p/k_l$.

CRM Preprint Series number 1152

The goal of this exercise is to define an 'equivalent fluid' with diffusivity α_e and from this infer the effective thermal conductivity k_e. This requires solving the system

$$\frac{\partial \theta_e}{\partial t} = \frac{\alpha_e}{r^2}\frac{\partial}{\partial r}\left(r^2\frac{\partial \theta_e}{\partial r}\right) \qquad \theta_e(1,t) = 1 \qquad \left.\frac{\partial \theta_e}{\partial r}\right|_{r=0} = 0\,. \tag{25}$$

This system is simple to solve, with a solution in terms of Bessel's functions. In particular the temperature at the centre is given by

$$\theta_e(0,t) = \theta_s(t) = 1 + \sum_{n=1}^{N} 2(-1)^n e^{-n^2\pi^2\alpha_e t}\,. \tag{26}$$

The system involving a particle is more difficult to deal with and so we rely on approximate solutions. First, note that to increase the thermal conductivity of a fluid nanoparticles are introduced with a much higher diffusivity than the base fluid. Typical values for copper and Al_2O_3 in water or ethylene-glycol solutions range from 60–1200 so $\alpha \gg 1$ and similarly $k \gg 1$. Effectively this means that heat is transferred much quicker through the particle than the fluid and we may set $T(r,t) \approx T_p(t)$. The thermal problem in the fluid may be reduced to a Cartesian system by setting $\theta = u/r$ and then the problem is identical to one treated by an accurate version of the Heat Balance Integral Method (HBIM) developed in [36, 37]. The HBIM permits simple polynomial approximations to the temperature in the fluid and particle and, more importantly, clearly shows the effect of the problem parameters. Integrating the heat equation over the domain leads to an ODE for the temperature T_p which then determines

$$T_p = 1 - e^{-\Lambda(t-t_1)}\,, \tag{27}$$

where $\Lambda = n\lambda/c_T$, $\lambda = 1/(1-r_p)^2$ and $c_T = (1+r_p)/2 - 1/(n+1)$. The time t_1 is when the temperature of the particle first rises, noticeably, above the initial temperature. The value $n = 2.233$ is determined in [36, 37] by minimising the least-squares error when the approximate solution is substituted into the heat equation.

Applying the HBIM to the equivalent fluid system leads to an expression for the centre temperature

$$T_c = 1 - e^{-\Lambda'(t-t_1')} \tag{28}$$

where $\Lambda' = n\alpha_e/c_{T0}$ and $c_{T0} = (n-1)/(2(n+1))$. We may verify the accuracy of the HBIM method by comparing the temperature predicted by equation (28) with that of (26). The result is shown in Figure 4. The HBIM solution predicts $T_c = 0$ until some time $t_1' > 0$ and then an exponential increase to the asymptote (which is scaled to 1). This follows the actual temperature $\theta_s(t)$ reasonably well.

Now the HBIM solution has been shown to be sufficiently accurate we may find an equivalent diffusivity by some form of matching of the HBIM solution with a particle and that for the equivalent fluid. In this case we take the simple option of equating the decay rates in the expressions for T_p and T_c (since this forces the temperature profiles

CRM Preprint Series number 1152

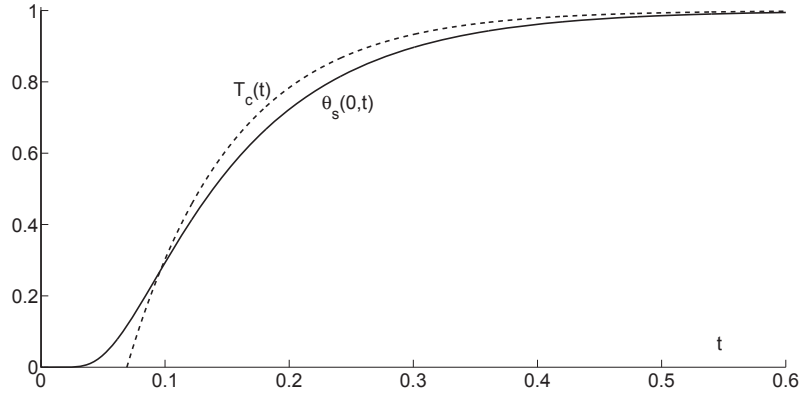

FIGURE 4. *Comparison of $T_c(t)$ and $\theta_s(t)$*

to be similar). This is equivalent to setting $\Lambda = \Lambda'$ which gives

$$\alpha_e = \frac{\alpha_l}{(1-r_p)^2}\frac{n-1}{2(n+1)}\left[\frac{1+r_p}{2} - \frac{1}{n+1}\right]^{-1}. \tag{29}$$

The radius r_p is non-dimensional, scaled with the fluid radius R. In general these types of relation are given in terms of the volume fraction ϕ where $r_p = \phi^{1/3}$,

$$\alpha_e = \frac{\alpha_l}{(1-\phi^{1/3})^2}\frac{n-1}{2(n+1)}\left[\frac{1+\phi^{1/3}}{2} - \frac{1}{n+1}\right]^{-1}. \tag{30}$$

Hence the thermal diffusivity of the equivalent fluid depends only on the liquid diffusivity and volume fraction (the value of $n = 2.233$ is fixed). The composition of the nanoparticle does not affect α_e. Noting that $\alpha_e = k_e/(\rho c)_e$ and $(\rho c)_e = \phi\rho_p c_p + (1-\phi)\rho_l c_l$, see [43], we may write the effective thermal conductivity as

$$\frac{k_e}{k_l} = \frac{\left[(1-\phi) + \phi\frac{\rho_p c_p}{\rho_l c_l}\right](n-1)}{(1-\phi^{1/3})^2\left[(1+\phi^{1/3})(n+1)-2\right]} \tag{31}$$

According to this formula, the equivalent particle conductivity is independent of the particle conductivity (this has been observed experimentally). The particle material enters through the density and specific heat $(\rho c)_p$, but since the ratio $\rho_p c_p/(\rho_l c_l)$ is order 1 and ϕ is small this is a weak dependence. Hence the effective conductivity is primarily a function of the liquid conductivity k_l and volume fraction ϕ.

The true test of a theory comes through comparison with experiment. In Figure 5 we compare the present prediction for k_e with that of Maxwell and a number of data sets taken from the literature for an Al_2O_3-water nanofluid, see [42]. As expected, there is quite a spread in the data and so we cannot hope to match all points. The prediction of the current theory, given by equation (31), is shown as the solid line, the Maxwell result of equation (20) is the dashed line. For very low volume fractions the Maxwell

CRM Preprint Series number 1152

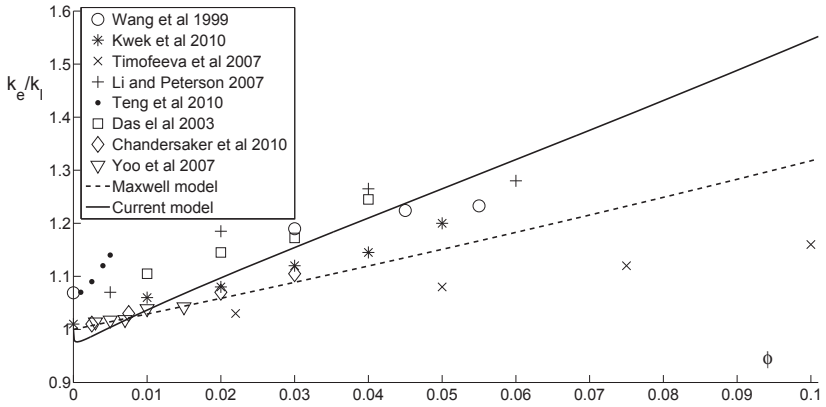

FIGURE 5. Conductivity ratio k_e/k_l for Al_2O_3-water nanofluid with $k_l = 0.58$W/mK: equation (31) (solid line); Maxwell model equation (20) (dashed line) and experimental data.

curve lies above the prediction of (31) and captures the data better, but for $\phi > 0.008$ (i.e. a volume fraction around 0.8% the present model rapidly increases above Maxwell and, more importantly, passes between a large amount of the experimental data. It is clear that the present model provides a much better approximation to the majority of experimental data when compared to the basic Maxwell model for volume fractions approximately greater than 1%.

5. CONCLUSION

In this paper we have briefly described three problems of current interest to the nano community. Although clearly we are working at the limit of continuum theory in each case the continuum models show good agreement with experimental results and provide valuable insight. Conversely, the nanoscale modelling can also provide valuable insight for macroscale problems. There is currently no theory for calculating slip length when a liquid moves over a solid surface. The study of flow in carbon nanotubes led to an expression for the slip length in terms of the depletion layer thickness and viscosity of the available gas. The study of nanofluids led to an expression for thermal conductivity for solid in liquid suspensions derived in a distinct way to the classical Maxwell model and valid for higher particle concentrations.

REFERENCES

[1] P. Abragall and N-T Nguyen. Nanofluidics. Artech House 2009.
[2] N-T. Nguyen and S.T. Werely. Fundamentals and applications of microfluidics. 2nd Edition, Artech House 2006.
[3] G. Guisbiers *et al*. J. Phys. Chem. C, 112:4097–4103, 2008.
[4] K.P. Travis *et al*. Phys. Rev. E, 55(4):4288–4295, 1997.
[5] C. Cottin-Bizonne *et al*. Rev. Lett., 94:056102, 2005.

CRM Preprint Series number 1152

[6] J.A. Thomas *et al*. Int. J. Therm. Sci., 49:281289, 2010.
[7] R. Kofman *et al*. Euro. Phys. J. D., 9(1-4), 441-444, 1999.
[8] C.-L. Kuo and P. Clancy. J. Phys. Chem. B, 109, 13743–13754, 2005.
[9] S.K. Das et al. Nanofluids: Science and Technology, Wiley 2007.
[10] J.K. Holt *et al*. Science 312:1034 2006, doi:10.1126/science.1126298.
[11] M. Majumder *et al.* Nat. Biotechnol., 438:44 2005.
[12] M. Whitby *et al*. Nanoletters, 8(9):2632–2637, 2008.
[13] F.M. White Viscous fluid flow. McGraw-Hill, New York 1991.
[14] J.A. Thomas and A.J.H. McGaughey. Nano Lett., 8(9):2788-2793, 2008.
[15] H. Verweij *et al*. Small 3(12):1996-2004. doi:10.1002/smll.200700368.
[16] A. Poynor Phy. Rev. Lett., 97:266101, 2006.
[17] C. Cottin-Bizonne et al. Phys. Rev. Lett., 94:056102, 2005.
[18] J.C.T. Eijkel and A. van den Berg. Microfluid Nanofluid, 1:249-267, 2005 doi: 10.1007/s10404-004-0012-9
[19] C. Neto *et al*. Rep. Prog. Phys., 68:28592897, 2005.
[20] M.T. Matthews and J.M. Hill. Int. J. Nanotechnol., 5(2/3):218-242, 2008.
[21] S. Joseph and N.R. Aluru. Nano Lett., 8(2):452-458, 2008.
[22] C-H Choi *et al*. Phys Fluids 15(10):2897-2902, 2003.
[23] J-L. Barratand L. Bocquet. Faraday Discuss. 112:119-27, 1999.
[24] H. Ye *et al*. Nanoscale Research Letters., 6:87, 2011.
[25] S. Karmakar et al. J. Phys.: Conf. Ser., 292:012002, 2011, doi:10.1088/1742-6596/292/1/012002.
[26] F. Ahmad *et al*. J. Nanopart. Res., 14:1038, 2012, DOI: 10.1007/s11051-012-1038-7.
[27] J.-H. Shim *et al*. Surf. Sci., 512:262–268, 2002.
[28] P. Bergese *et al*. J. Phys. Chem. B, 108:15488–15493, 2004.
[29] S. Rana *et al*. Adv. Drug. Delivery Rev., 64:200–216, 2012.
[30] S. W McCue et al. Proc. Roy. Soc. A, 464(2096):2055–2076, 2008.
[31] J. Buongiorno *et al.* J. Appl. Phys., 106:094312, 2009.
[32] R. Prasher *et al*. Phys. Rev. Lett., 94:025901, 2005.
[33] J. Koo and C. Kleinstreuer.J. Nanopart. Res., 6:577-588, 2004.
[34] W. Yu and S.U.S. Choi. J. Nanopart. Res. 5:167–171, 2003.
[35] T.G. Myers Microfluid. Nanofluid. 2010. DOI: 10.1007/s10404-010-0752-7.
[36] T.G. Myers. Int. Comm. Heat Mass Trans., 36(2):143–147, 2009. DOI:10.1016/j.icheatmasstransfer. 2008.10.013.
[37] T.G. Myers. Int. J. Heat Mass Trans., 2010.
[38] F. Font *et al*. Submitted to J. Nanopar Res., 2013.
[39] Ph. Buffat *et al*. Phys Rev A, 13(6):2287–2298, 1976.
[40] X. Liu *et al* Mat. Chem. Phys., 10: 1–4, 2007.
[41] P. Keblinski *et al*. J. Nanopart Res., 10:1089-1097, 2008.
[42] T.G. Myers *et al*. Sumitted to J. Nanopar Res., 2013.
[43] S.Q. Zhou and N. Rui. Appl. Phys. Lett., 92:093123, 2008.

T.G. MYERS
CENTRE DE RECERCA MATEMÀTICA
CAMPUS DE BELLATERRA, EDIFICI C
08193 BELLATERRA, BARCELONA, SPAIN
TEL.: +34-935868517
FAX: +34-935812202
E-mail address: tmyers@crm.cat

CRM Preprint Series number 1152

M.M. MACDEVETTE
CENTRE DE RECERCA MATEMÀTICA
CAMPUS DE BELLATERRA, EDIFICI C
08193 BELLATERRA, BARCELONA, SPAIN
DEPARTAMENT DE MATEMÀTICA APLICADA I
UNIVERSITAT POLITÈCNICA DE CATALUNYA
BARCELONA, SPAIN
E-mail address: mmacdevette@crm.cat

F. FONT
CENTRE DE RECERCA MATEMÀTICA
CAMPUS DE BELLATERRA, EDIFICI C
08193 BELLATERRA, BARCELONA, SPAIN
DEPARTAMENT DE MATEMÀTICA APLICADA I
UNIVERSITAT POLITÈCNICA DE CATALUNYA
BARCELONA, SPAIN
E-mail address: ffont@crm.cat

CRM Preprint Series number 1152

CRM
CENTRE DE RECERCA MATEMÀTICA
Facultat de Ciències, UAB
08193 Bellaterra
Barcelona, Spain
www.crm.cat